# Heterostructure engineered construction of N-doped CuO@$Co_3O_4$ for highly efficient electrocatalytic reduction of nitrate to ammonia

Shi-Jiao Dong, Sai Huang, Ao Wang, Yan Meng, Gang Xu and Jun-Ling Song*

International Joint Research Center for Photoresponsive Molecules and Materials, School of Chemical and Material Engineering, Jiangnan University, Lihu Street 1800, Wuxi 214122, China

## Experimental section

**Materials:** All chemical reagents were purchased from commercial suppliers and were used as received without further purification. Methyl Alcohol, Ammonium Formate, Cobalt(II) nitrate hexahydrate ($Co(NO_3)_2 \cdot 6H_2O$) and Copper(II) nitrate trihydrate ($Cu(NO_3)_2 \cdot 3H_2O$) were purchased from Shanghai Titan Scientific Co., Ltd. Sodium nitrate ($NaNO_3$, 99.0%), sodium nitrite ($NaNO_2$, 99.0%), ammonium chloride ($NH_4Cl$), potassium dihydrogen phosphate ($KH_2PO_4$,99%), were purchased from Sinopharm Chemical Reagent Co., Ltd. Commercial NF was purchased from Suzhou Cheng Er Nuo Technology Co. Ltd. Fragments of nickel foam with an effective area of $1 \times 1$ cm$^2$ were first washed with ethanol and acetone for 15 min with the help of ultrasound. The nickel foam flakes were then immersed in 6 M HCl solution for 15 min and finally washed with distilled water and acetone before use. Deionized (DI) water is homemade in a laboratory.

### Synthesis of $Cu_2(OH)_3(NO_3)$ /NF

For the preparation of $Cu_2(OH)_3(NO_3)$/NF (CuHN/NF), a 50 mL autoclave containing 5 g of $Cu(NO_3)_2 \cdot 3H_2O$ was transferred into an oven at 140 °C for 20 min till the salt was totally melted. Then the pretreated NF pieces were dipped into the molten salt and reacted at 140 °C for 15 min.

### Synthesis of N-doped CuO@$Co_3O_4$/NF

Specifically, the electrodeposition was carried out at a constant potential of -1.0 V (vs. saturated calomel electrode, SCE) for 600 s in a standard three-electrode system, with CuHN/NF and Calomel electrode as working and counter electrode, respectively. The electrolyte consisted of 0.1 M $Co(NO_3)_2$. The consequent precursor was then rinsed and vacuum-dried, followed by annealing at 350 °C for 3 h with a heating rate of 5 °C min-1 in an air atmosphere.

### Synthesis of R-CuHN/NF

In particular, the electrochemical in-situ reduction on the basis of CuHN/NF yields to $Cu_{2+1}O$/NF (R-CuHN/NF).

### Synthesis of $Cu(OH)_2$/NF

R-CuHN/NF immersion the reaction was left to stand for 15 minutes in an aqueous solution containing 4 mL of 0.5 M $(NH_4)_2S_2O_8$, 8 mL of 5 M NaOH, and 9 mL of deionized water, followed by removal and rinsing with deionized water and absolute ethanol before transferring dry in a 60 °C constant temperature oven for later use.

Synthesis of $Cu_{2+1}O@Co_3O_4$/NF

Specifically, the $Cu_2(OH)$/NF and calomel electrodes are used exclusively as working and counter electrodes, and the electrodeposited was carried out in 0.1 M $Co(NO_3)_2$ aqueous solution, followed by the low-temperature calcination as described above.

Synthesis of $Co_3O_4$/NF

Specifically, the Ni foam and calomel electrodes are used exclusively as working and counter electrodes, and and the electrodeposited was carried out in 0.1 M $Co(NO_3)_2$ aqueous solution, followed by the low-temperature calcination as described above.

Synthesis of N-doped CuO/NF

CuHN/NF is then annealed at 350 °C for 3 h in an air atmosphere at a heating rate of 5 °C min-1, and then N-doped CuO/NF.

**Characterizations:** XRD data were acquired by Brukef D8 instrument with Cu-Kα radiation; SEM measurements were carried out on a Hitachi S-4800 Scanning Electron microscope. TEM images were collected on a JEOL JEM 2100F electron microscopy. XPS spectra were recorded on a Kratos AXIS Ultra $^{DLD}$ X-ray photoelectron spectrometer. An electron paramagnetic resonance spectrometer (EPR, Bruker A300) was used for electron spin resonance (ESR) measurements. ICP-OES was measured in Thermo Fisher iCAP PRO. UV-Vis absorbance spectra were obtained on a PERSEE TU-1950 spectrophotometer. $^1$H NMR spectra were acquired on a Bruker Avance NEO 600 MHz. Electron paramagnetic resonance (EPR) spectra were acquired on a Bruker EMXplus-6/1 spectrometer at room temperature.

**Electrochemical measurements:** All electrochemical measurements were performed in an H-type cell separated by a treated ion exchange membrane Nafion 117 using the CHI760E electrochemical workstation (Shanghai, Chenhua) with a standard three-electrode setup. The electrolyte solution was 0.1 M PBS with an additional 50 mM $NaNO_3$, using N-doped $CuO@Co_3O_4$/NF as the working electrode, saturated calomel electrode (SCE) as the reference electrode, Pt foil (1cm$^2$) as the counter electrode and the prepared catalyst as the working electrode with an effective working area of 1 cm ×1 cm. Before testing, cyclic voltammetry scanning of the working electrode is performed until the signal is stable. The scan rate for linear sweep voltammetry is 10 mV s$^{-1}$. The Potentiostatic tests were performed at a specific potential (-0.35, -0.45, -0.55, -0.65, -0.75, -0.85and -0.95 V vs.RHE) for 1 hour at a fixed speed of 400 rpm. All potentials reported in our work were converted to a reversible hydrogen electrode (RHE) scale and the current density was normalized by the geometrical area of the electrode (1 cm$^2$).

**Detection of ammonium-N:** The $NH_3$ concentration was quantitatively determined by Nessler's reagent. Firstly, 0.2 mL of electrolyte was taken out from the cathode cell and diluted to 50 mL in the colorimetric tube. Then, Sodium potassium tartrate solution (1 mL) and Nessler's reagent (1 mL) were added sequentially. After shaking well and standing for 10 minutes, the absorbance was tested by UV-Vis spectrophotometry at a wavelength of 420 nm. The concentration-absorption spectra were calibrated using standard $NH_4Cl$ solution with different concentrations.

**Detection of nitrate-N:** Firstly, 0.2 mL electrolyte was taken out from the cathode cell and diluted to 50 mL in the colorimetric tube. Then, 1 mL 1 M HCl and 0.1mL 0.8 wt% sulfamic acid solution were added in turn into the aforementioned solution. Finally, the absorbance of the as-prepared mixture was detected by UV-Vis spectrophotometry at a wavelength of 220 nm and 275 nm. The concentration-absorption spectra were calibrated using standard $KNO_3$ solution with different concentrations.

**Detection of nitrite-N:** Firstly, 0.2 mL electrolyte was taken out from the cathode cell and diluted to 50 mL in the colorimetric tube. 1 mL of color reagent was sequentially added. After shaking well and standing for 20 minutes, the absorbance at 540 nm was then measured by a UV-Vis spectrophotometer. The concentration-absorption spectra were calibrated using a standard $NaNO_2$ solution with different concentrations (Figure S3). The color developer was prepared as follows:20 g of p-amino benzenesulfonamide was dissolved in the mixed solution of water (250 mL) and phosphoric acid (50 ml). Then 1 g of N-(1-naphthyl)-ethylenediamine dihydrochloride was added to the above mixture. Finally, the above solution was diluted to 500 mL after being transferred to a flask.

**Determination of $NH_3$ yield and FE:**

$$\text{Faradaic efficiency} = (8F \times C_{NH3} \times V)/(M_{NH3} \times Q) \times 100\%$$

$$NH_3 \text{ yield} = (C_{NH3} \times V) / (t \times S)$$

Where $C_{NH3}$ was the concentration of products, $V$ was the volume of cathodic electrolyte, $F$ was the Faraday constant (96,485 C $mol^{-1}$), $M$ was the molar mass of products, $Q$ was the total quantity of applied electricity, $t$ was the electrolysis time, and $S$ was the geometric area of working electrode ($1\times1$ $cm^2$).

**$NO_3^-$ isotopic labeling experiment**: The generated $^{15}NH_4^+$ and $^{14}NH_4^+$ were verified by isotope-labelled tracer experiments using 50mM $Na^{15}NO_3$ and $Na^{14}NO_3$ as nitrogen sources, respectively. After 1 h of chronoamperometry test at –0.95V vs RHE, the pH of the post-electrolysis electrolyte was adjusted to 1~ 2 with 4 M $H_2SO_4$. Then, the electrolyte (500 μL) was mixed with DMSO-d6 (50 μL) for further $^1H$ NMR detection.

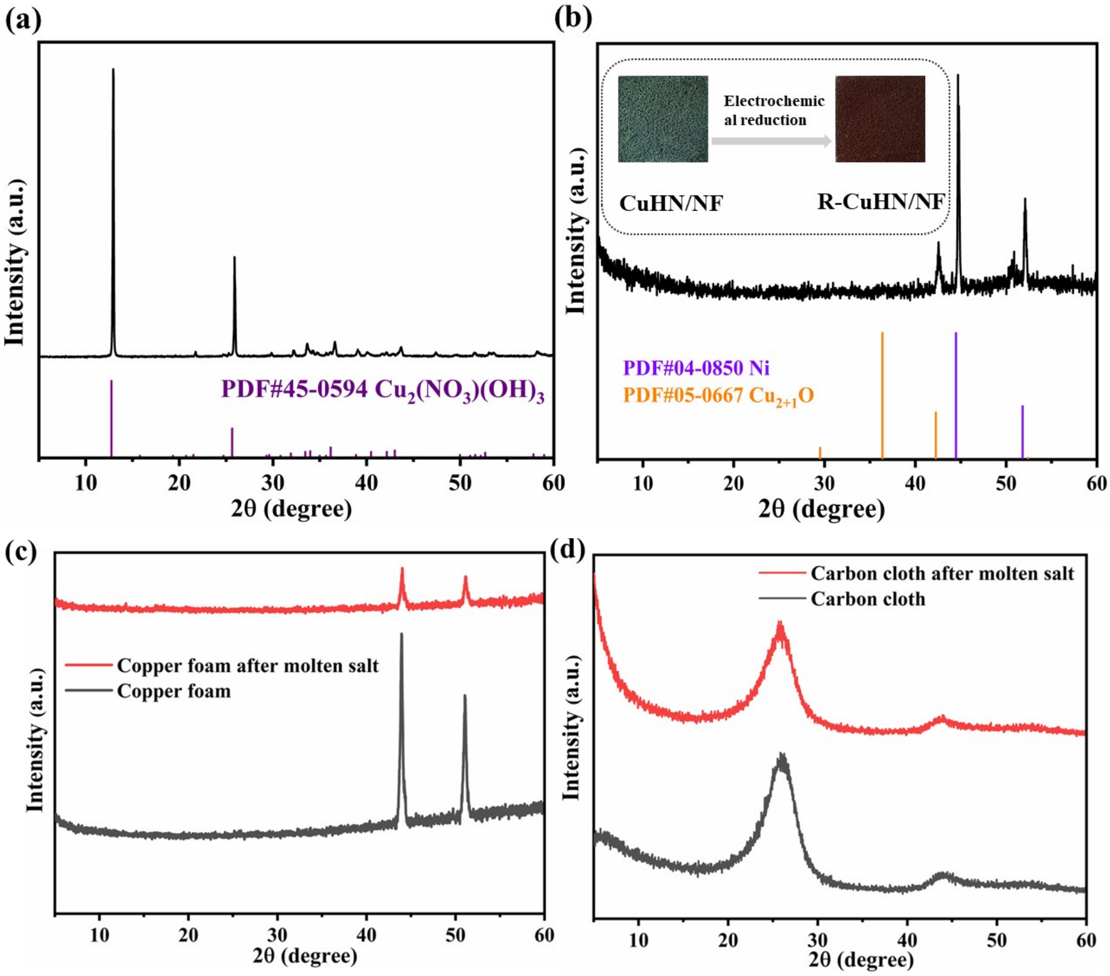

**Fig. S1.** PXRD patterns of (a) $Cu_2(NO_3)(OH)_3$/NF and (b) $Cu_{2+1}O$/NF (c) Copper foam and Copper foam after loading $Cu_2(NO_3)(OH)_3$ molten salt (d) carbon cloth and carbon cloth after molten salt.

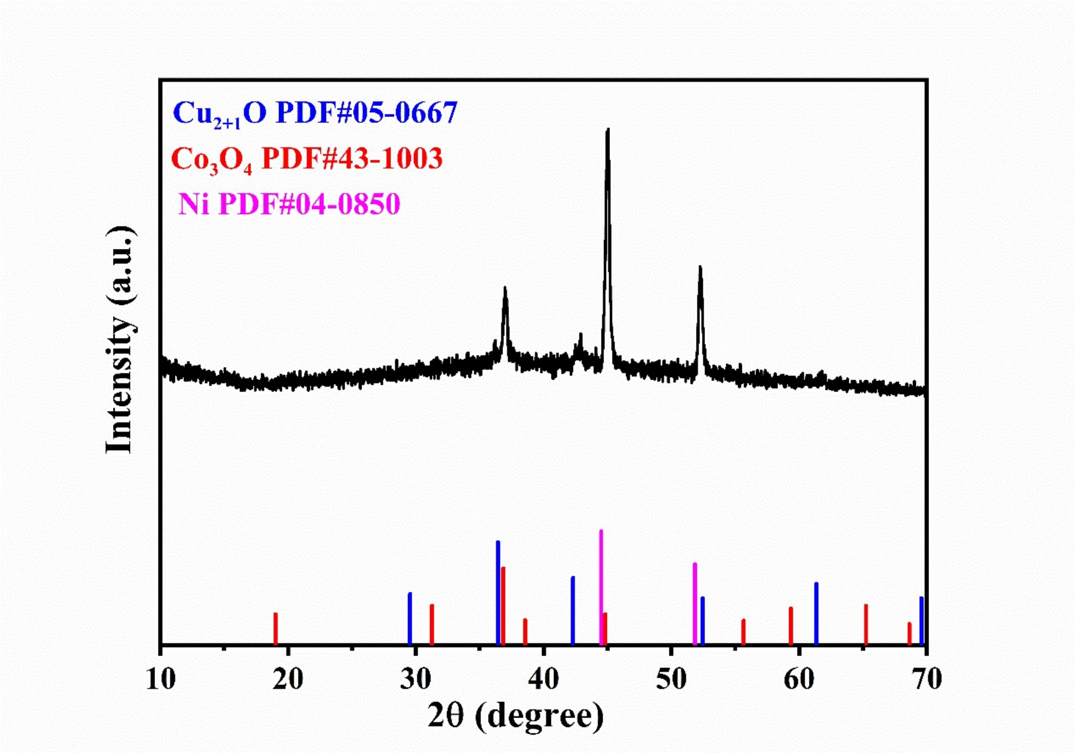

**Fig. S2. (a)** PXRD patterns of $Cu_{2+1}O$@$Co_3O_4$/NF.

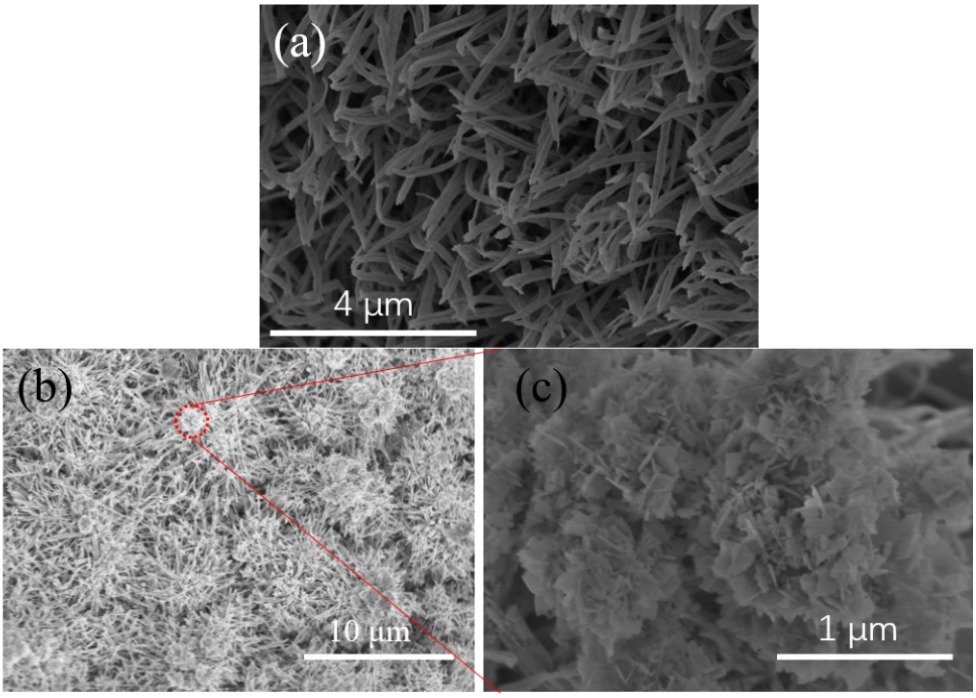

**Fig. S3.** SEM images (a) Cu $(OH)_2$/NF and (b-c) $Cu_{2+1}O@Co_3O_4$/NF

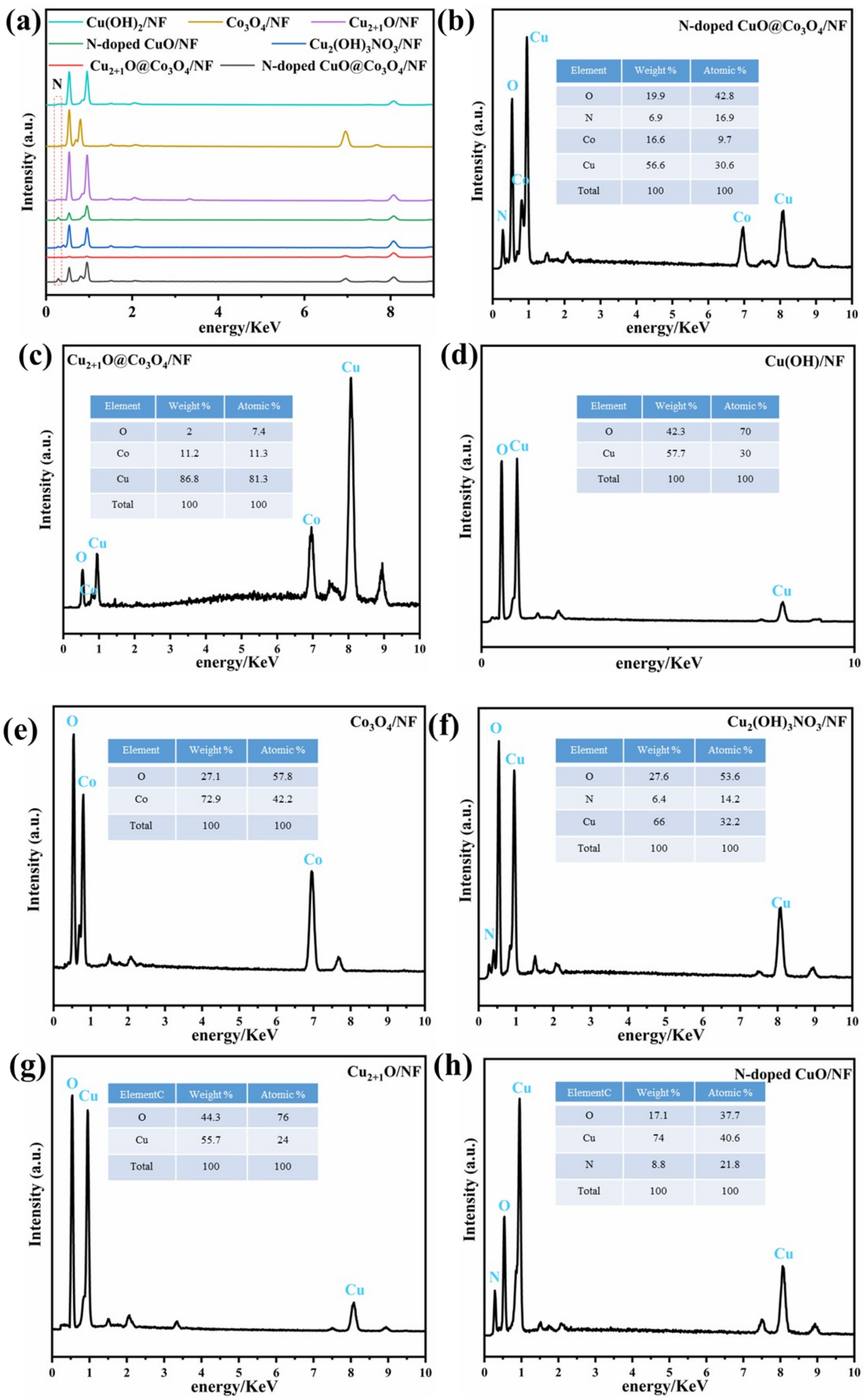

(b)

| Element | Weight % | Atomic % |
|---|---|---|
| O | 19.9 | 42.8 |
| N | 6.9 | 16.9 |
| Co | 16.6 | 9.7 |
| Cu | 56.6 | 30.6 |
| Total | 100 | 100 |

(c)

| Element | Weight % | Atomic % |
|---|---|---|
| O | 2 | 7.4 |
| Co | 11.2 | 11.3 |
| Cu | 86.8 | 81.3 |
| Total | 100 | 100 |

(d)

| Element | Weight % | Atomic % |
|---|---|---|
| O | 42.3 | 70 |
| Cu | 57.7 | 30 |
| Total | 100 | 100 |

(e)

| Element | Weight % | Atomic % |
|---|---|---|
| O | 27.1 | 57.8 |
| Co | 72.9 | 42.2 |
| Total | 100 | 100 |

(f)

| Element | Weight % | Atomic % |
|---|---|---|
| O | 27.6 | 53.6 |
| N | 6.4 | 14.2 |
| Cu | 66 | 32.2 |
| Total | 100 | 100 |

(g)

| ElementC | Weight % | Atomic % |
|---|---|---|
| O | 44.3 | 76 |
| Cu | 55.7 | 24 |
| Total | 100 | 100 |

(h)

| ElementC | Weight % | Atomic % |
|---|---|---|
| O | 17.1 | 37.7 |
| Cu | 74 | 40.6 |
| N | 8.8 | 21.8 |
| Total | 100 | 100 |

**Fig. S4**. EDX images of O, N, Co, and Cu in (a)Total; (b) N-doped CuO@$Co_3O_4$/NF; (c) $Cu_{2+1}O@Co_3O_4$/NF; (d) Cu(OH)/NF (e) $Co_3O_4$/NF; (f) $Cu_2(OH)_3NO_3$/NF; (g) $Cu_{2+1}O$/NF; (h) N-doped CuO/NF.

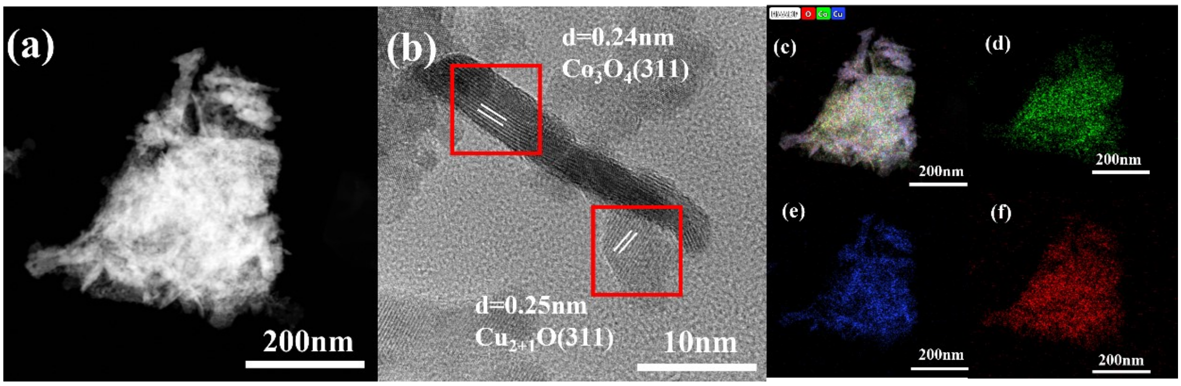

**Fig. S5.** $Cu_{2+1}O@Co_3O_4$/NF (a) TEM images; (b) High-resolution transmission electron microscope (HR-TEM) images; (c) EDS element distribution map; (d-f) Mapping images of corresponding elements Co, Cu and O.

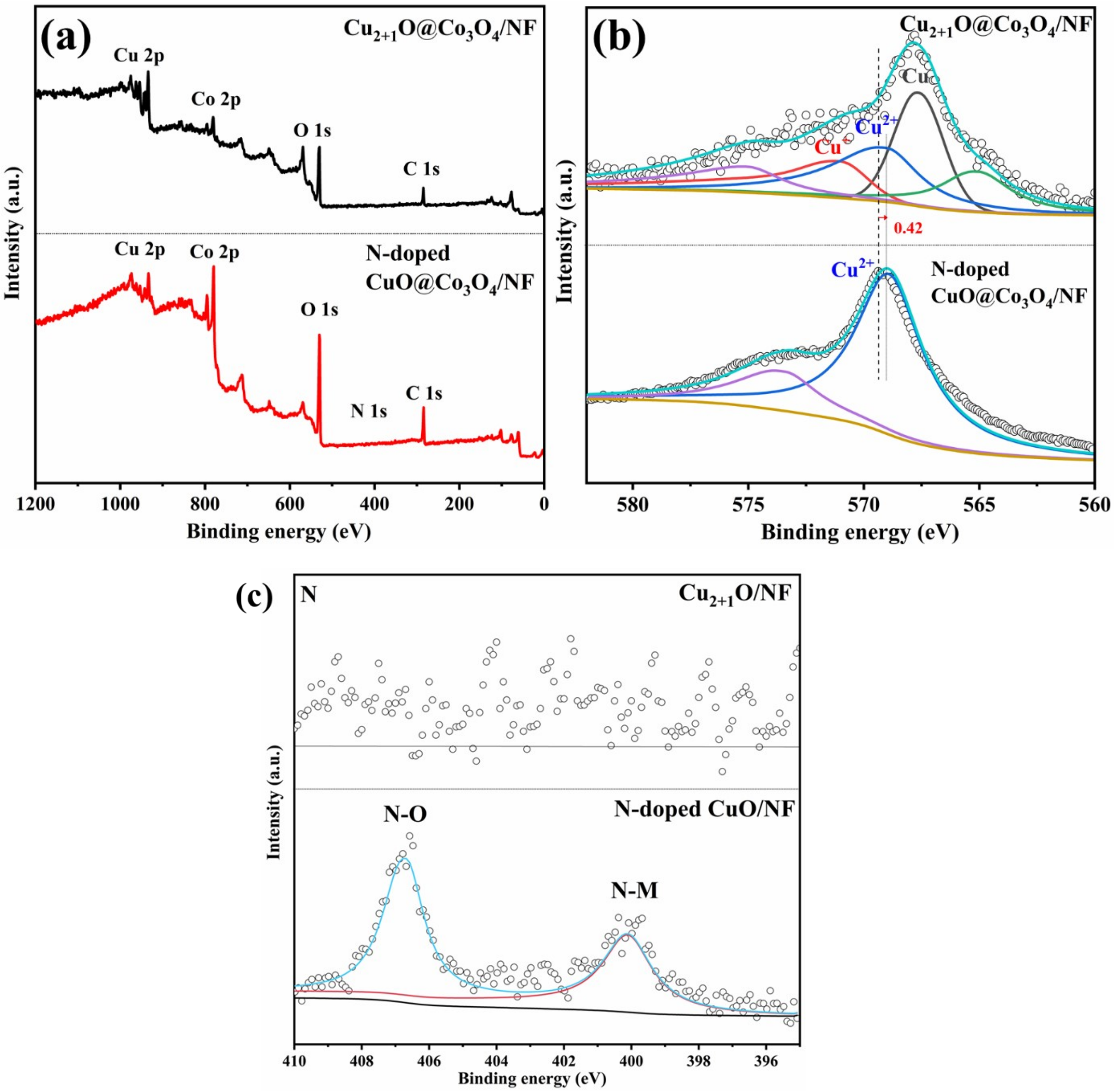

**Fig.S6** High-resolution XPS spectra for N-doped CuO@Co$_3$O$_4$/NF and Cu$_{2+1}$O@Co$_3$O$_4$/NF, (a) survey; (b) Auger spectra of Cu; (c) Spectra of N in N-doped CuO/NF and Cu$_{2+1}$O/NF.

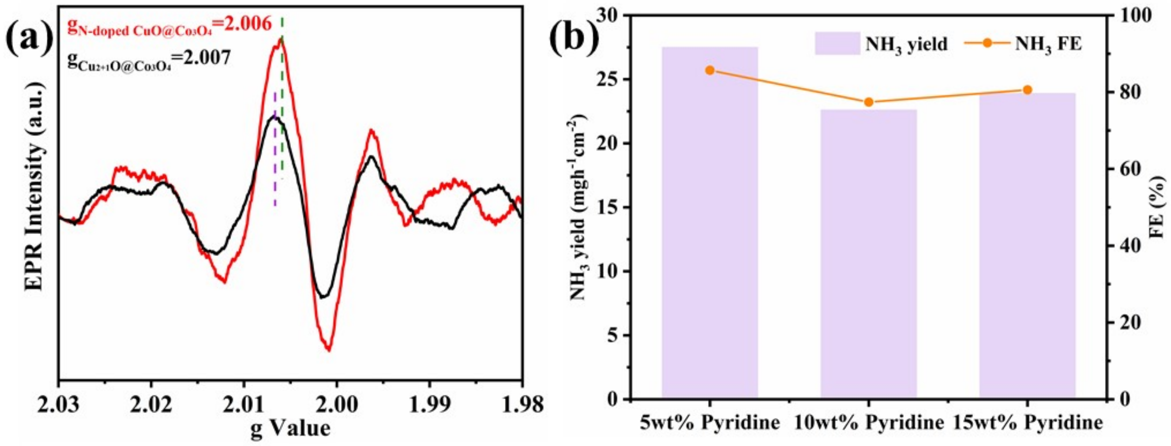

**Fig. S7**. (a) EPR spectrum of N-doped CuO@Co$_3$O$_4$/NF and Cu$_{2+1}$O@Co$_3$O$_4$/NF**;** (b) Effect of pyridine on the yield and Faraday efficiency of N-doped CuO@Co$_3$O$_4$/NF.

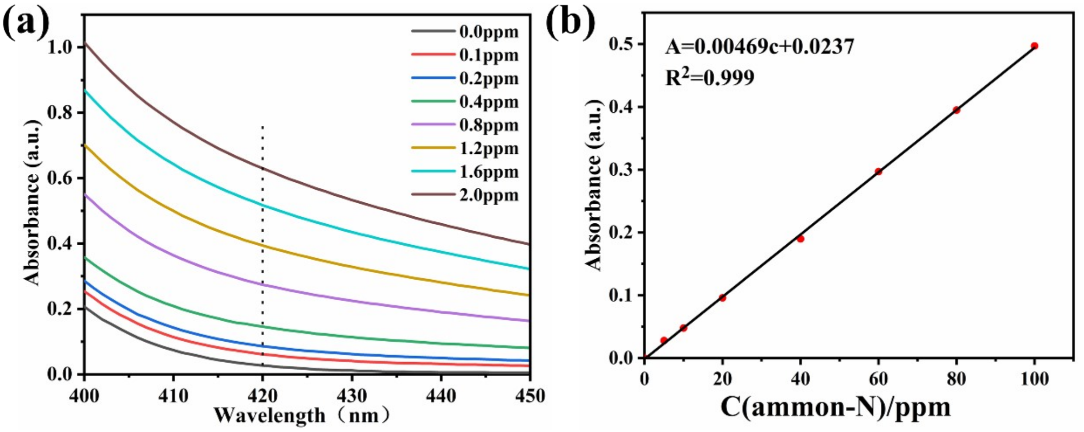

**Fig. S8**. (a) UV-Vis absorption spectra and (b) corresponding calibration curve used for calculation of $NH_4^+$-N concentration.

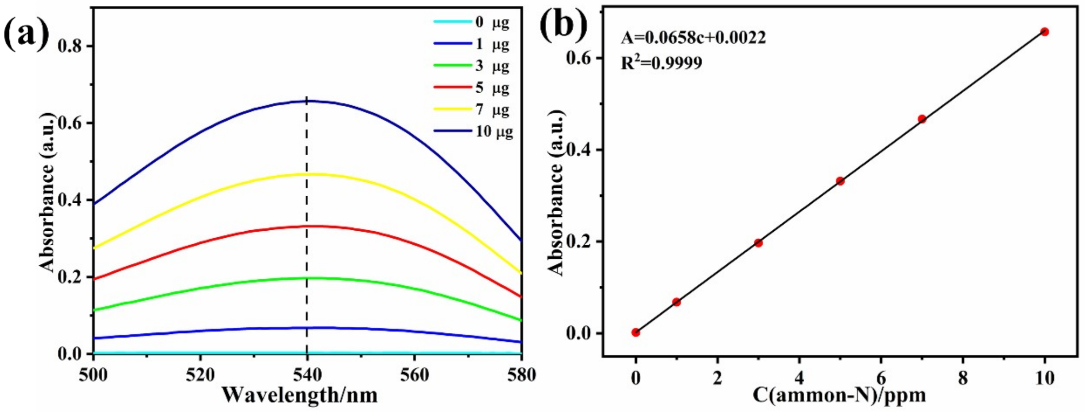

**Fig. S9**. (a) UV-Vis absorption spectra and (b) corresponding calibration curve used for calculation of $NO_2^-$-N concentration.

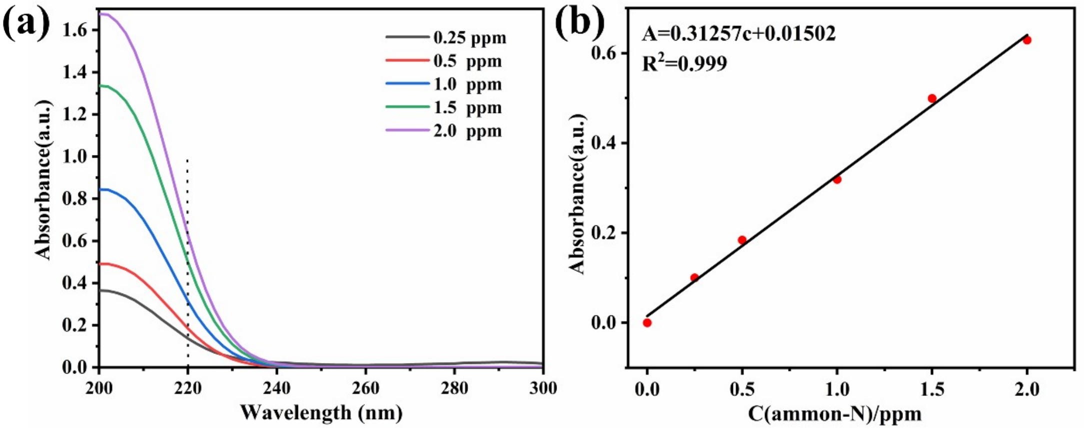

**Fig. S10**. (a) UV-Vis absorption spectra and (b) corresponding calibration curve used for calculation of $NO_3^-$-N concentration.

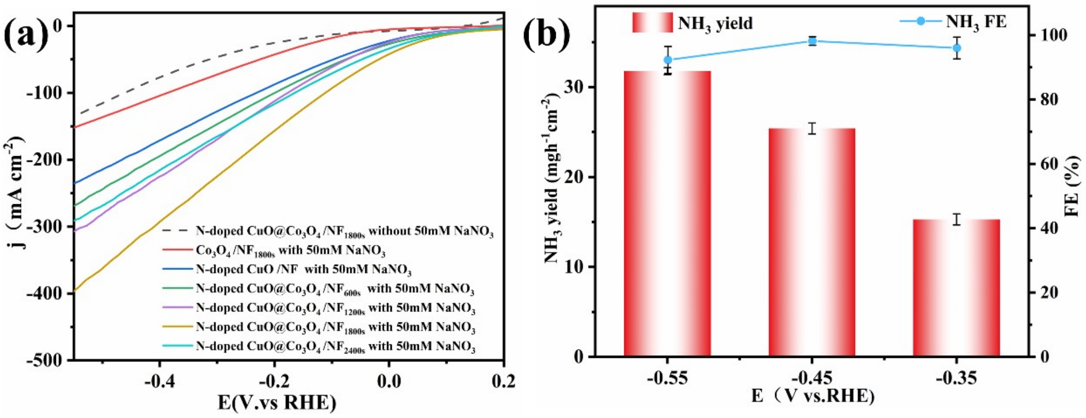

**Fig. S11.** (a) LSV curves of N-doped CuO/NF, $Co_3O_4$/NF, N-doped CuO@$Co_3O_4$/NF (600s, 1200s, 1800s, 2400s) measured in 0.1 M PBS without/with at 50 mM $NaNO_3$; (b) N-doped CuO@$Co_3O_4$/NF1800s FE and ammonia yield, the error bar represents the range of results from three independent measurements.

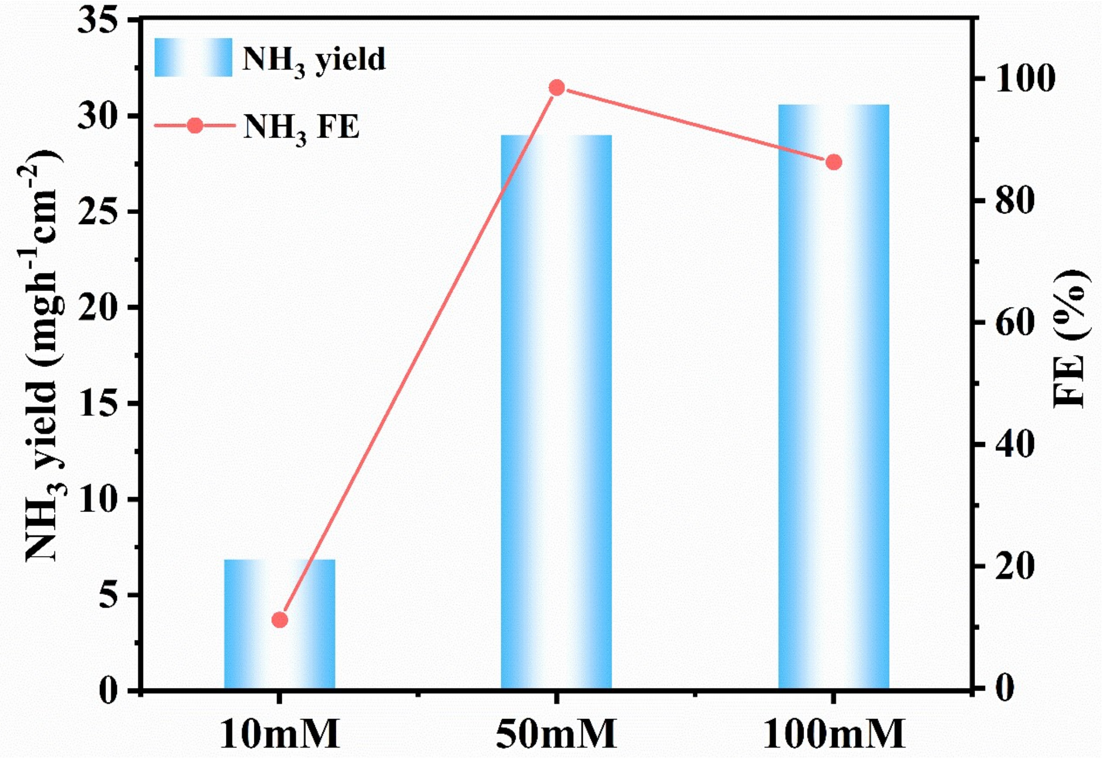

**Fig. S12**. $NH_3$ yield and FE comparisons were tested at -0.85 V for N-doped $CuO@Co_3O_4$/NF and in 0.1M PBS electrolytes containing 10, 50 and 100 mM $NaNO_3$.

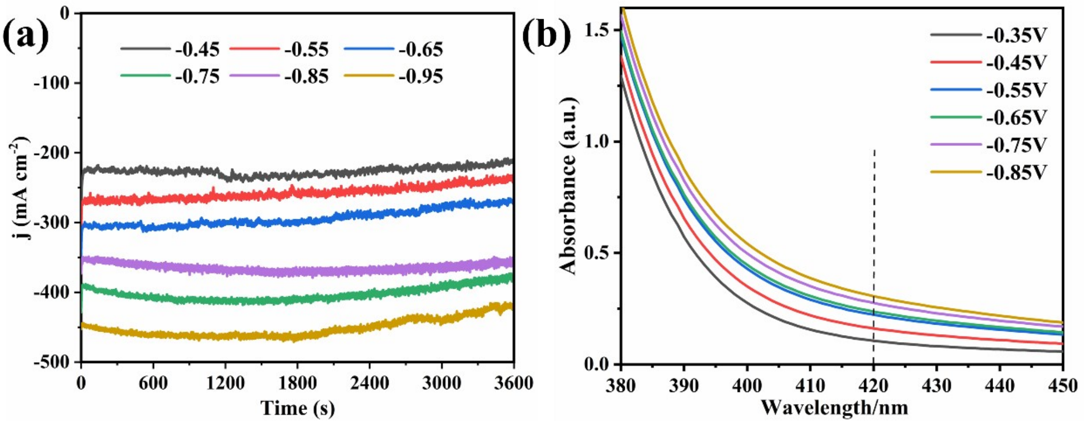

**Fig. S13.** (a) Chronoamperometry curves and (b) corresponding UV-Vis absorption of N-doped CuO@$Co_3O_4$/NF in the 0.1 M PBS with 50 mM $NaNO_3$ at different applied potentials.

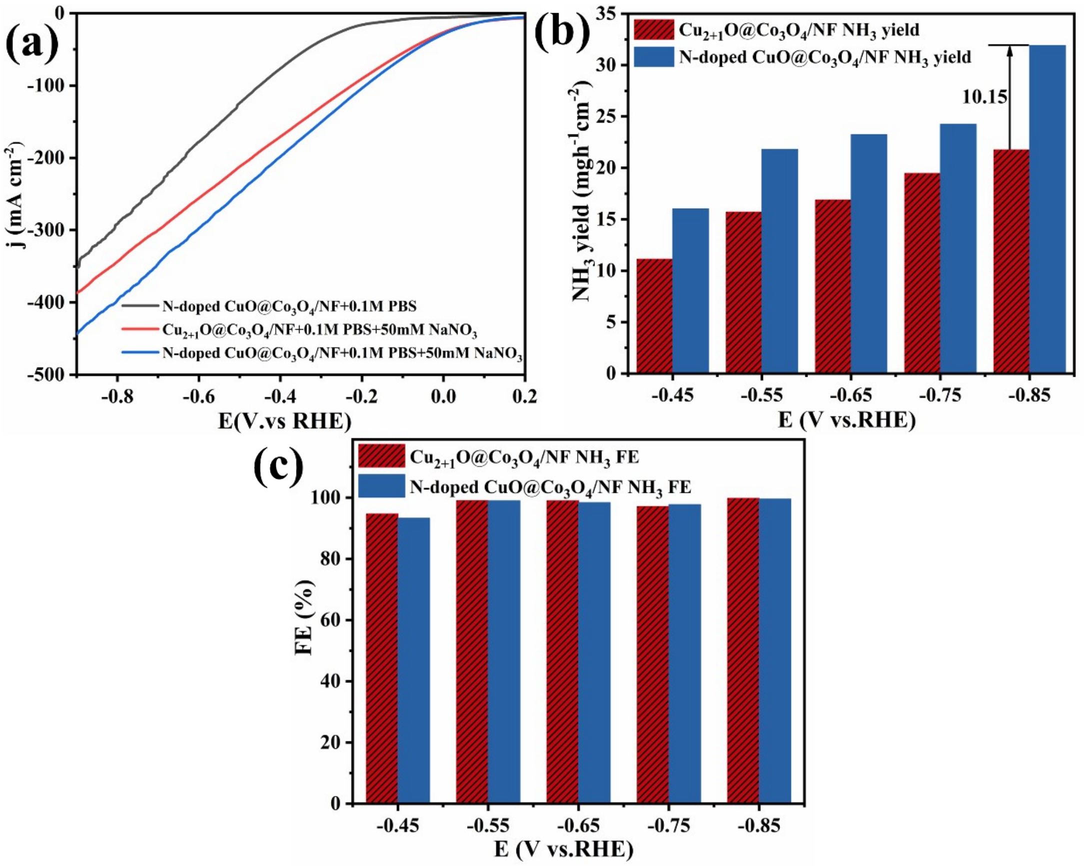

**Fig. S14**. (a) LSV curves of N-doped CuO@$Co_3O_4$/NF and $Cu_{2+1}O$@ $Co_3O_4$/NF measured in 0.1 M PBS with/without 50 m M $NaNO_3$; (b) $NH_3$ yields of N-doped CuO@$Co_3O_4$/NF and $Cu_{2+1}O$@$Co_3O_4$/NF at different potentials; (c) $NH_3$ FE of N-doped CuO@$Co_3O_4$/NF and $Cu_{2+1}O$@$Co_3O_4$/NF at different potentials.

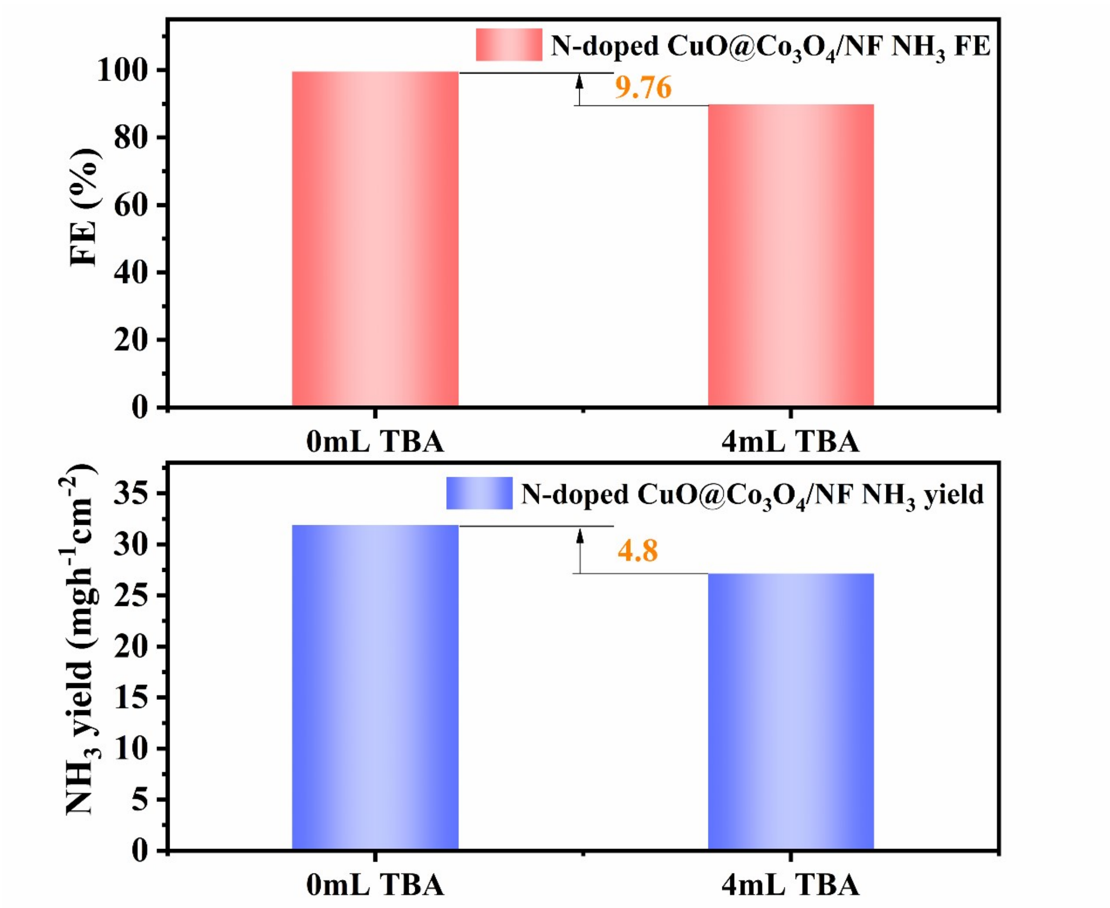

**Fig. S15.** Effect of TBA (tert-butanol) on N-doped CuO@Co$_3$O$_4$/NF yield and Faraday efficiency.

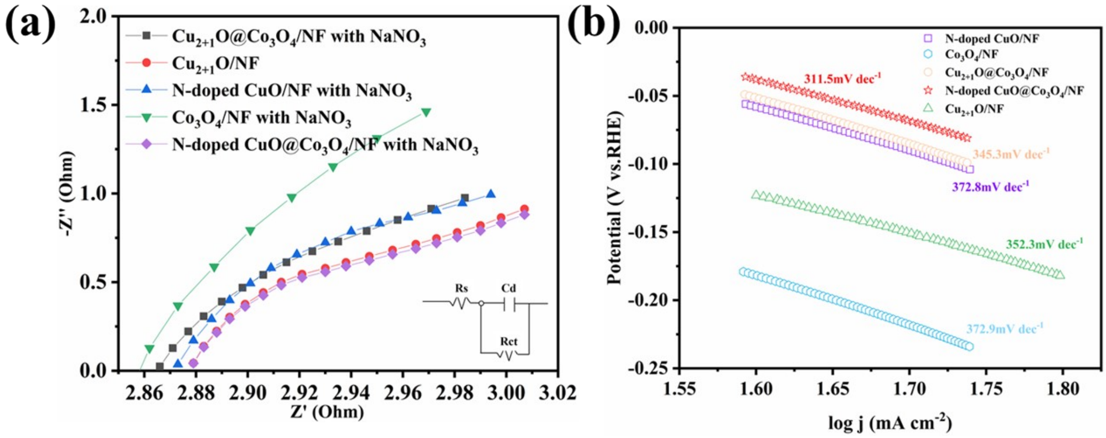

**Fig. S16.** (a) Corresponding Nyquist diagram: The inset is the Tafel slope corresponding to the equivalent circuit diagram; (b) Tafel slope for N-doped-CuO/NF, $Co_3O_4$/NF, N-doped CuO@$Co_3O_4$/NF, $Cu_{2+1}O$@$Co_3O_4$/NF and $Cu_{2+1}O$/NF.

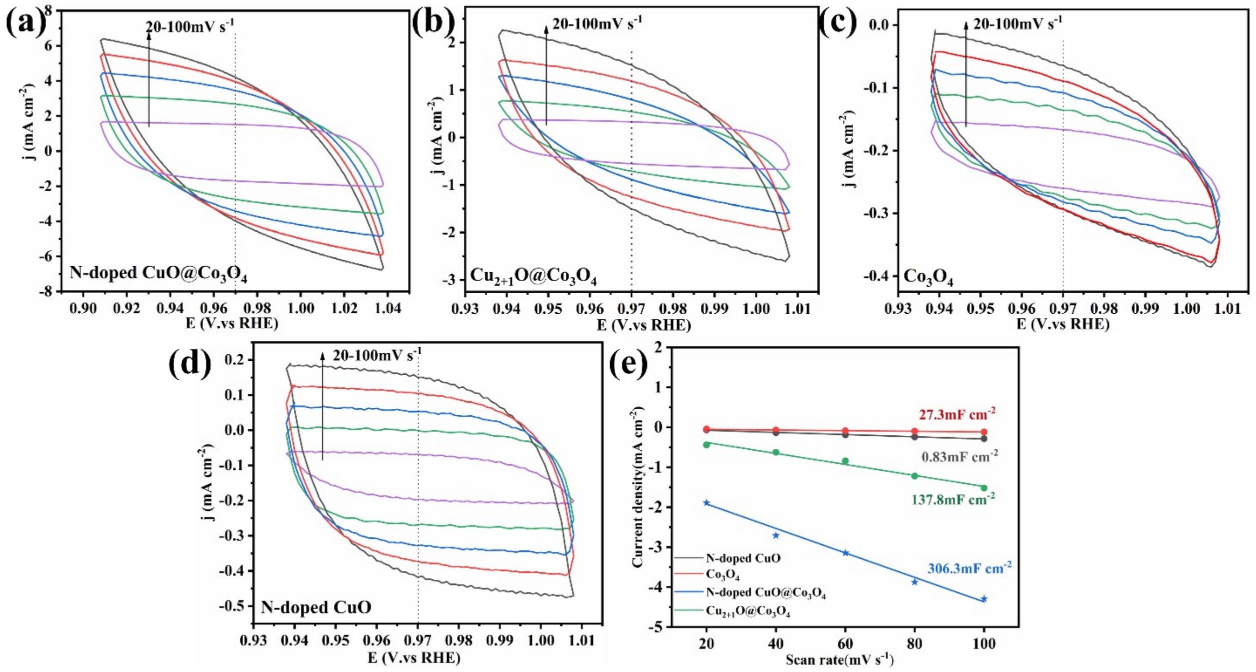

**Fig. S17.** Cyclic voltamperes at scan rates of 20-100mV $s^{-1}$ (a) N-doped CuO@$Co_3O_4$/NF; (b) $Cu_{2+1}O$@$Co_3O_4$/NF; (c) $Co_3O_4$/NF; (d) N-doped CuO; (e) The relationship between current density and scan rate corresponding to 0.97 V (vs. Hg/HgO).

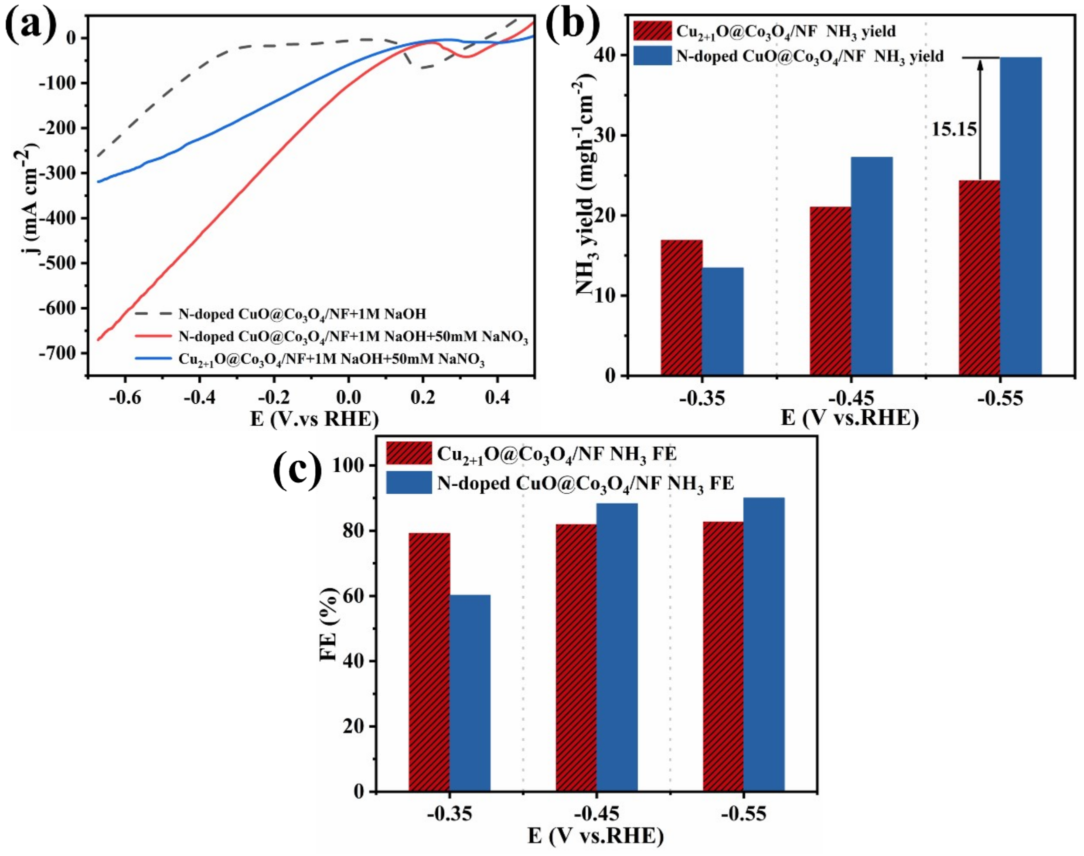

**Fig. S18**. (a) LSV curves of N-doped CuO@Co$_3$O$_4$/NF and Cu$_{2+1}$O@ Co$_3$O$_4$/NF measured in 1 M NaOH with/without 50 m M NaNO$_3$; (b) NH$_3$ yields of N-doped CuO@Co$_3$O$_4$/NF and Cu$_{2+1}$O@Co$_3$O$_4$/NF at different potentials; (c) NH$_3$ FE of N-doped CuO@Co$_3$O$_4$/NF and Cu$_{2+1}$O@Co$_3$O$_4$/NF at different potentials.

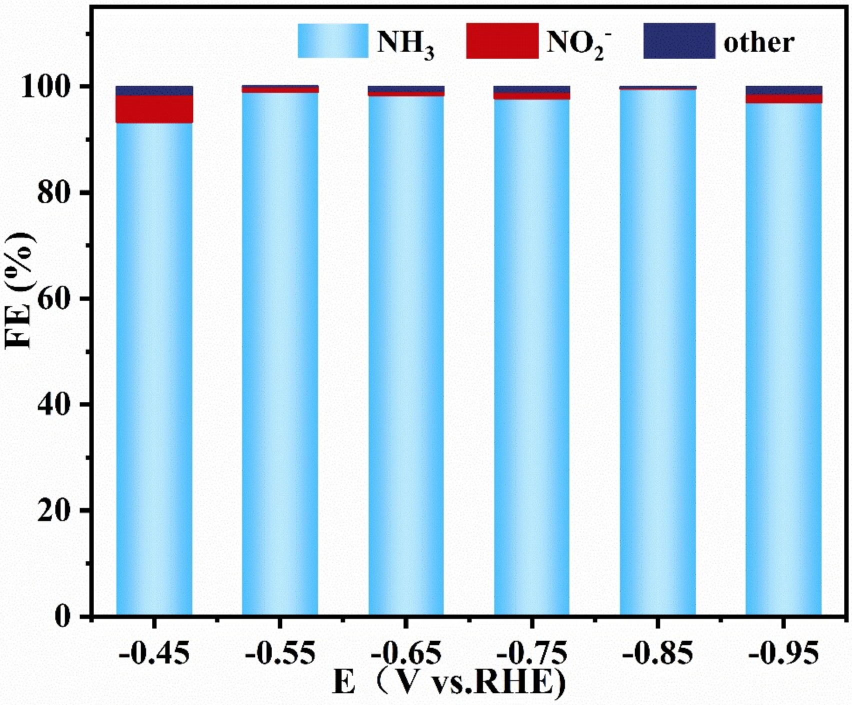

**Fig. S19** Product distribution of N-doped CuO@Co$_3$O$_4$/NF between -0.45 and -0.95 V.

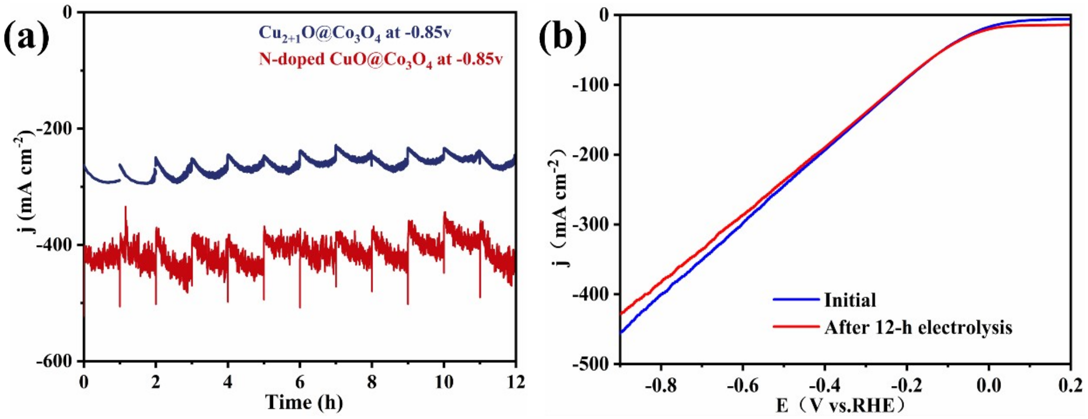

**Fig. S20.** (a) Chronoamperometry curve of N-doped CuO@$Co_3O_4$/NF and $Cu_{2+1}O$@$Co_3O_4$/NF at −0.85 V for 12 h; (b) LSV curves before and after stabilization of N-doped CuO@$Co_3O_4$/NF cycles.

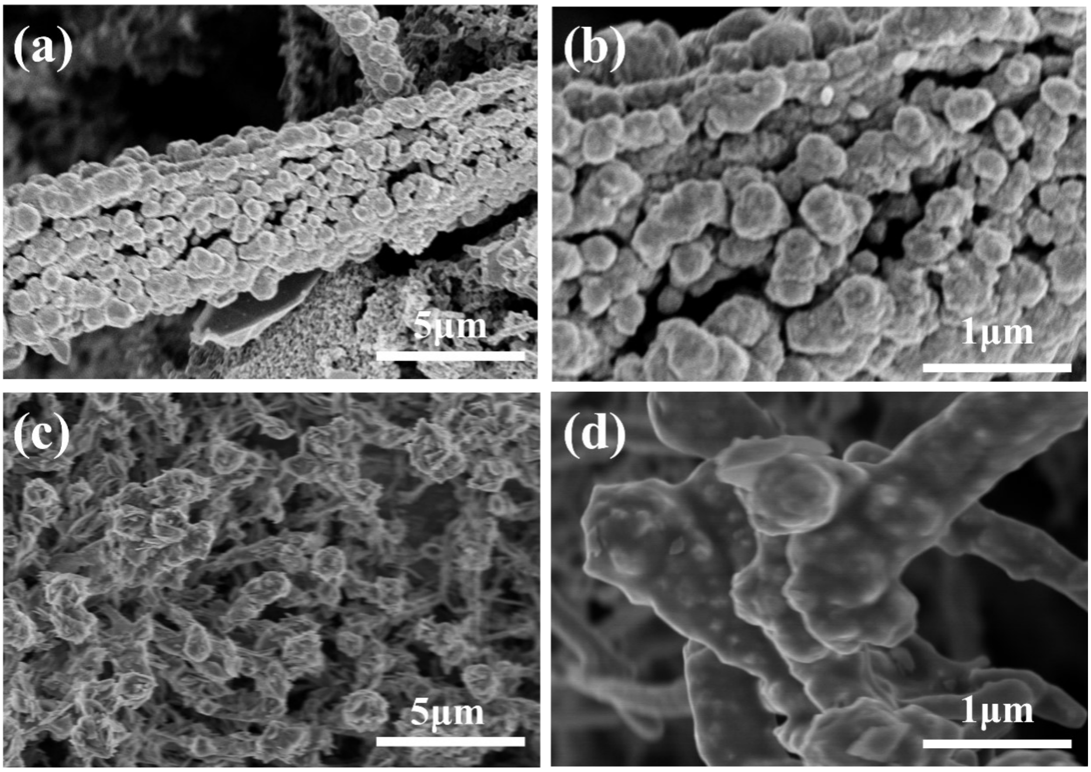

**Fig. S21.** SEM images for (a-b) N-doped CuO@$Co_3O_4$/NF and (c-d) $Cu_{2+1}O$@$Co_3O_4$/NF after long-time electrolysis.

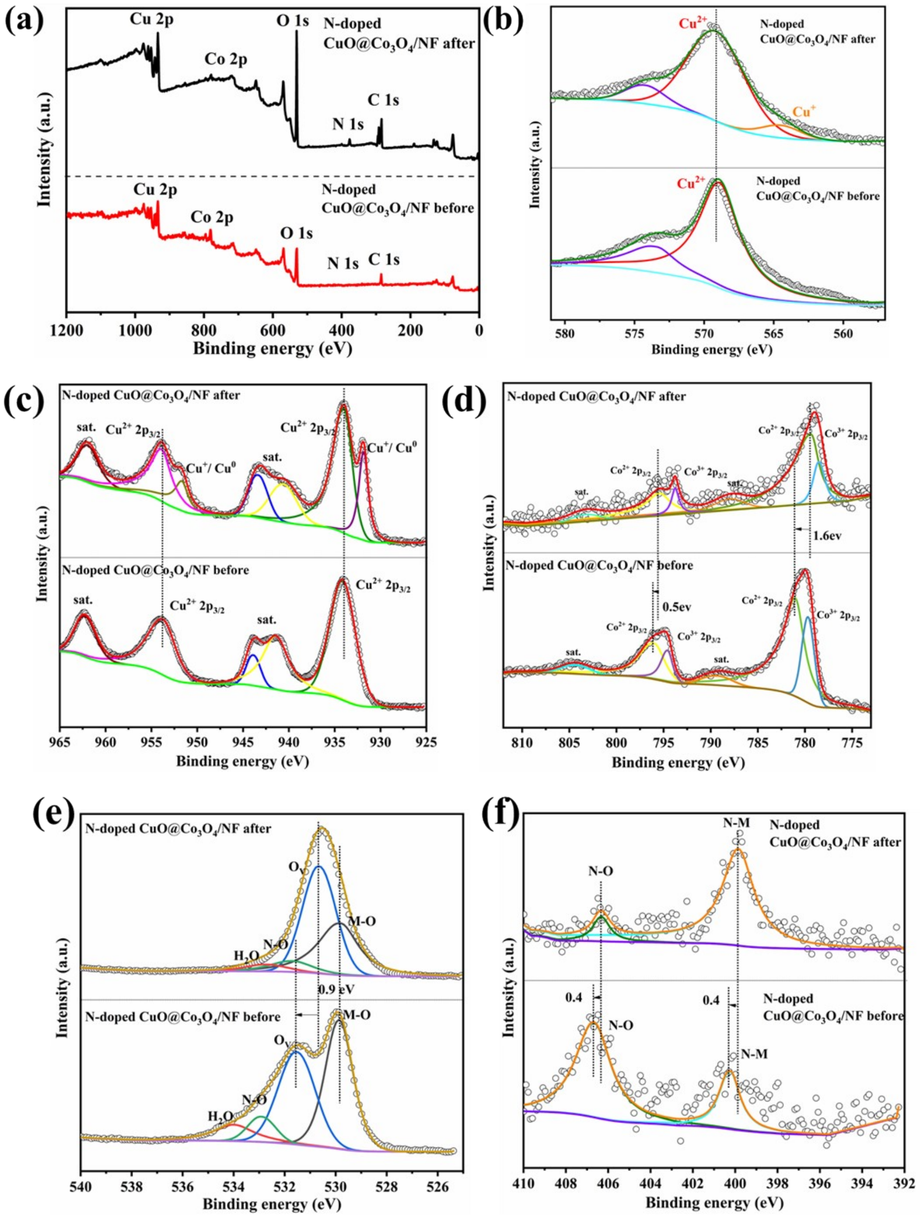

**Fig.S22.** High-resolution XPS spectra for N-doped CuO@Co$_3$O$_4$/NF before and after 12 h of the eNO$_3$RR test, (a) survey; (b) Auger spectra of Cu; (c) Cu 2p; (d) Co 2p; (e) O 1s; (f) N 1s.

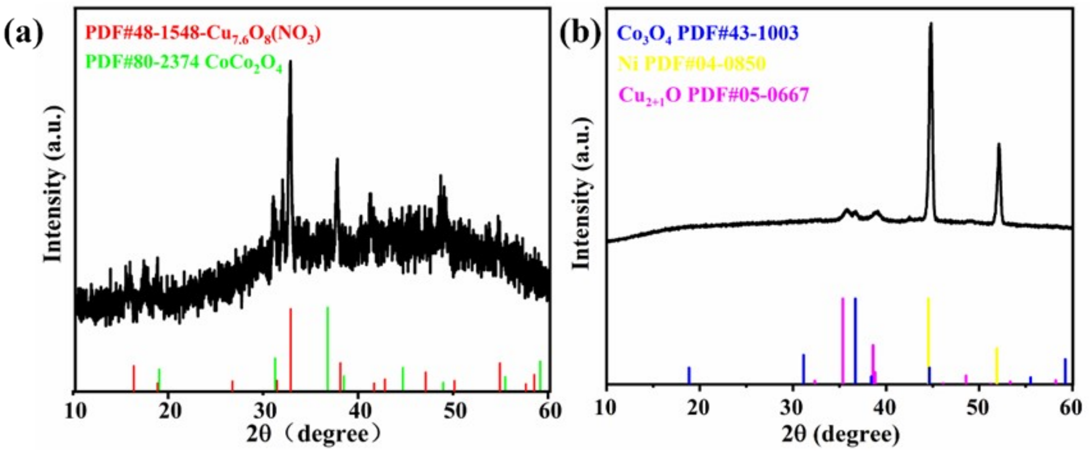

**Fig. S23.** XRD pattern for (a) N-doped CuO@$Co_3O_4$/NF and (b) $Cu_{2+1}O$@$Co_3O_4$/NF after long-time electrolysis.

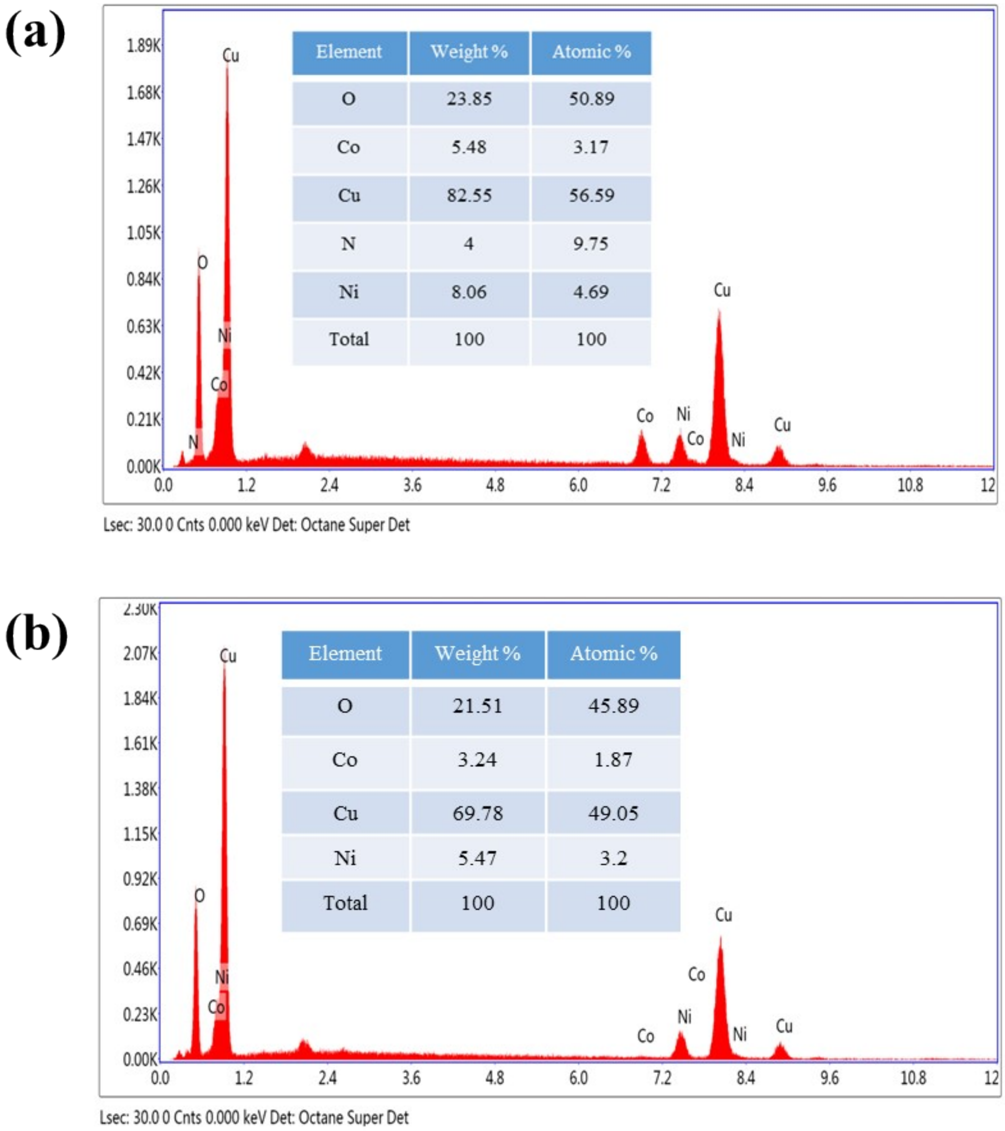

(a)

| Element | Weight % | Atomic % |
|---|---|---|
| O | 23.85 | 50.89 |
| Co | 5.48 | 3.17 |
| Cu | 82.55 | 56.59 |
| N | 4 | 9.75 |
| Ni | 8.06 | 4.69 |
| Total | 100 | 100 |

(b)

| Element | Weight % | Atomic % |
|---|---|---|
| O | 21.51 | 45.89 |
| Co | 3.24 | 1.87 |
| Cu | 69.78 | 49.05 |
| Ni | 5.47 | 3.2 |
| Total | 100 | 100 |

**Fig. S24.** EDX spectra of the (a) N-doped $CuO@Co_3O_4$/NF and (b) $Cu_{2+1}O@Co_3O_4$/NF long-time electrolysis.

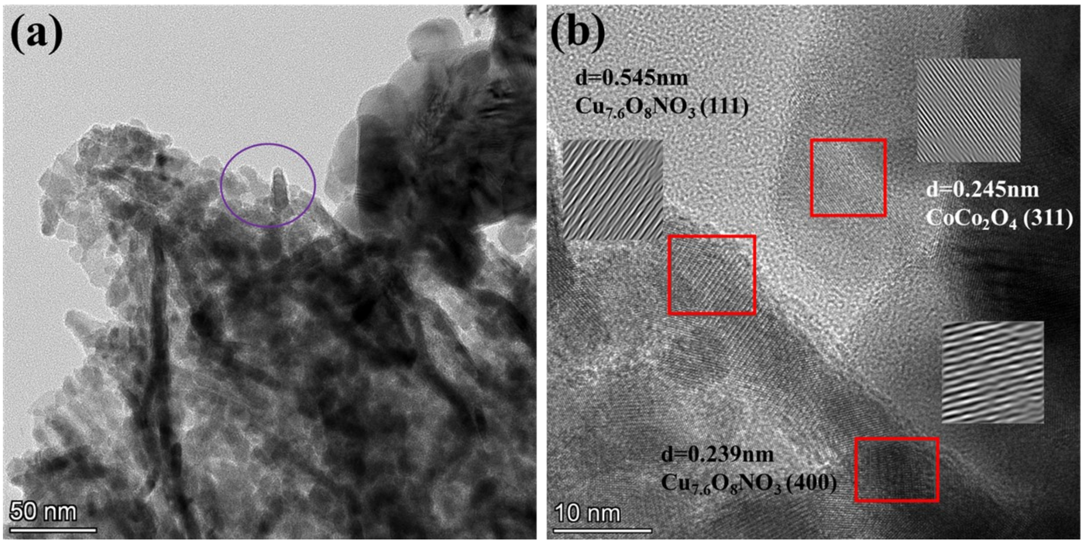

**Fig. S25.** N-doped CuO@$Co_3O_4$/NF after long-time electrolysis (a) TEM images; (b) High-resolution transmission electron microscope (HR-TEM) images.

Table S1. The content of Co and Cu in N-doped CuO@$Co_3O_4$/NF according to three times Inductively Coupled Plasma (ICP) measurement.

| **Catalyst** | **Test element** | **Test solution element concentration Co (mg/L)** | **Sample element content $C_x$ (mg/kg)** | **Sample element content W (%)** |
|---|---|---|---|---|
| N-doped CuO@$Co_3O_4$/NF | Co | 1.65 | 62123.49 | 6.21 |
| | Co | 1.649 | 62085.84 | 6.21 |
| | Co | 1.655 | 62311.75 | 6.23 |
| | Cu | 16.185 | 609375.00 | 60.9 |
| | Cu | 16.182 | 609262.05 | 60.9 |
| | Cu | 16.117 | 606814.76 | 60.7 |

Table S2. The Co element content in the as-prepared hetero-structure with different electrodeposition times.

| **Catalyst** | **Electrodeposition time (s)** | **Co Weight (%)** |
|---|---|---|
| **$Cu_{2+1}O@Co_3O_4$** | **600** | **13.61** |
| **$CuO@Co_3O_4$** | **0** | **0** |
| | **600** | **11.65** |
| | **1200** | **14.02** |
| | **1800** | **22.85** |
| | **2400** | **26.73** |

Table S3. Comparison of catalytic performance of the as-prepared hetero-structure in this work with other reported non-noble-metal e$NO_3$RR catalysts.

| Catalyst | Electrolyte | FE (%) @ E (V vs RHE) | $NH_3$ yield (mg/h/cm$^2$) | Refs. |
|---|---|---|---|---|
| N-doped CuO@$Co_3O_4$/NF | 0.1M PBS (50 mM $NO_3^-$) | 99.51 (-0.85 V) | 31.92(-0.85 V) | This work |
|  | 1M NaOH (50 mM $NO_3^-$) | 90.2 (-0.55V) | 39.65 (-0.55V) | This work |
| $Cu_{2+1}O$@$Co_3O_4$/NF | 0.1M PBS (50 mM $NO_3^-$) | 99.78 (-0.85 V) | 21.37(-0.85 V) | This work |
|  | 1M NaOH (50 mM $NO_3^-$) | 82.7 (-0.55V) | 24.35 (-0.55V) | This work |
| $Fe_3O_4$/SS | 0.1 M NaOH (0.1 M $NO_3^-$) | 91.5 (-0.5 V) | 10.15 (-0.5 V) | Nano Res., **2021**, 15, 3050 |
| $ZnCo_2O_4$ NSA/CC | 0.1 M NaOH (0.1 M $NO_3^-$) | 98.33 (-0.6 V) | 10.79 (-0.8 V) | Mater. Today Phys., **2022**, 23, 100619 |
| Cu–PTCDA | 1 M PBS (500 ppm $NO_3^-$) | 77 (-0.4 V) | 0.44 (-0.4 V) | Nat.Energy, **2020**, 5, 605 |
| Ce–$MoS_{2-x}$/CC | 0.5 M $Na_2SO_4$ (0.1 M $NO_3^-$) | 96.6 (-0.7 V) | 7.3 (-0.9 V) | Inorg.Chem.Front., **2023**,10, 1543 |
| CuCl BEF | 0.5 M $Na_2SO_4$ (100 mg/L $NO_3^-$) | 88 (-1 V) | 1.82 (-1 V) | Angew. Chem. Int. Ed., **2021**, 60, 22933 |
|  | 0.5 M $K_2SO_4$ |  |  | Angew. Chem. Int. |

| | | | | |
|---|---|---|---|---|
| | | | | Ed., **2022**,134, e202114538 |
| N-doped CuO NWAs | 0.5 M $Na_2SO_4$<br>(200 ppm $NO_3^-$) | 95.8(-0.85 V) | 4.16 (-0.85 V) | Angew. Chem. Int. Ed., **2020**, 59, 5350 |
| CF@$Cu_2O$ | 0.1 M PBS<br>(0.1 M $NO_2^-$) | 94.21 (-0.6 V) | 7.51 (-0.6 V) | Chem. Commun., **2022**, 58, 517 |
| Fe-$SnS_2$/CC | 0.5 M $Na_2SO_4$<br>(0.1 M $NO_3^-$) | 85.6 (-0.7 V) | 7.2 (-0.8 V) | Dalton Trans.,**2022**,51,10343 |